

Quantifying Plio-Pleistocene Global Mean Sea Level Variation

F. D. Richards^{a,*}

^a*Department of Earth Science & Engineering, Imperial College London, South Kensington, London, SW7 2BP, UK*

Abstract

Future sea-level rise poses an imminent threat to coastal communities and actionable sea-level forecasts are urgently needed to ensure they are adequately protected. Such projections cannot be developed without deep understanding of the mechanisms driving sea-level change and how they responded in the past to climatic forcings akin to those expected in the near future. Quantifying the amplitudes of Plio-Pleistocene sea-level highstands, and their correlation with other palaeoclimatic variables, is therefore of critical societal importance. Here, I review the geodynamic processes that complicate sea-level reconstructions and how associated ice volume estimates have evolved with improved understanding of these phenomena.

Keywords: Sea level, Dynamic Topography, Glacial Isostatic Adjustment, Geoid, Palaeoclimate, Mid-Pliocene Warm Period, Last Interglacial

Key Points

- Global mean sea level (GMSL) during past warm periods can only be determined from geomorphic records after careful correction for relative sea-level (RSL) changes caused by solid Earth processes.
- RSL variations caused by dynamic topography and glacial isostatic adjustment (GIA) are ubiquitous and are often of comparable magnitude to GMSL variations, making them especially important to constrain.
- Recent observational, theoretical, and computational advances allow these processes to be modelled with far greater accuracy, improving accuracy and uncertainty quantification of Plio-Pleistocene GMSL estimates.
- Revised understanding of past GMSL can significantly reduce the considerable uncertainties that currently exist in ice-sheet-model-based sea-level projections.

¹ 1. Introduction

² Deepening our understanding of the long-term relationship between sea-level and climate forcing is key to developing more accurate and actionable projections of future sea-level change. While
³ instrumental records yield direct and precise measurements of Earth's modern climatic evolution,
⁴

*Corresponding author

Email address: f.richards19@imperial.ac.uk (F. D. Richards)

5 they are generally brief (< 60 yrs) and may be of limited relevance to the more extreme environments
6 that could prevail in the near future, restricting their usefulness for inferring future trends.
7 Geological proxy records, although indirect and less complete, provide complementary constraints
8 on sea level and climate covariation over a broader range of conditions, helping to refine sea-
9 level forecasts on 10^1 – 10^2 yr timescales. Measurements from the most recent periods of enhanced
10 warmth and high *global mean sea-level* (GMSL) are especially valuable since these intervals rep-
11 resent the closest analogues to the near-future climate states. Considerable focus has therefore
12 been placed on reconstructing sea level and ice sheet configuration during the Mid-Pliocene Warm
13 Period (MPWP; \sim 3.3–3.0 Ma) and the Last Interglacial (LIG; \sim 129–116 ka), periods characterised
14 by global mean temperatures 2–3°C and \sim 1°C above preindustrial values, respectively.

15 GMSL variations since the onset of the Pliocene period, \sim 5.3 million years ago, have generally
16 been inferred using either temperature-corrected oxygen isotope compositions of foraminifera and
17 ostracods (often in conjunction with Mg/Ca ratios; Raymo et al., 2018), or elevations of geomorphic
18 sea-level indicators, such as palaeoshoreline deposits and backstripped sedimentary successions
19 (Miller et al., 2020). The former approach provides a continuous record of GMSL variation across
20 the past few million years, but is subject to considerable uncertainty due to analytical precision
21 limitations, difficulties discriminating between temperature and ice volume signals, and poorly
22 constrained diagenetic effects. These geochemically derived GMSL estimates are therefore accurate
23 to no better than $\sim \pm 15$ m (Raymo et al., 2018). Since these uncertainties are comparable to the
24 differences between present-day sea level and peak sea level during past warm periods, efforts to
25 quantify past highstand amplitudes have generally focused on palaeoshoreline records. While these
26 geomorphic proxies can potentially provide more accurate GMSL constraints, care must be taken
27 to account for processes that cause locally recorded *relative sea level* (RSL) changes to deviate
28 from globally averaged signals.

29 Here, I describe these physical mechanisms and review the characteristic magnitudes and
30 timescales of the RSL variations they produce. Next, advances in modelling and removing their
31 effects are discussed, as well as the impact these breakthroughs have had on our current under-
32 standing of major Pliocene-Recent highstands. Finally, outstanding challenges are summarised,
33 with suggestions offered for how best to leverage new data sets and modelling techniques to make
34 progress in these areas.

35 **2. Physical Drivers of Pliocene-to-Recent Relative Sea-Level Change**

36 Geomorphic proxies record changes in RSL, which is equivalent to the elevation difference be-
37 tween the solid Earth and the ocean surface. Processes that vertically perturb either boundary
38 can therefore cause RSL to deviate from GMSL (the area-weighted mean of RSL), and these dis-
39 placements must be accurately quantified before sea-level markers can be used to infer ice volumes.
40 Over short timescales (10^{-2} – 10^1 years), local RSL variations of up to a metre can be caused by
41 ocean dynamics ('dynamic ocean topography'), subsidence due to groundwater depletion, and ma-
42 jor earthquakes. However, on the longer timescales (10^4 – 10^6 years) relevant to Plio-Pleistocene
43 warm periods, several additional mechanisms start to dominate the RSL signal: glacial isostatic
44 adjustment (GIA; i.e., sea-level and topography variations caused by ice and ocean mass changes);
45 mantle dynamic topography (i.e., vertical deflections of Earth's solid surface driven by mantle con-
46 vection); sustained tectonic activity; erosion and sedimentation (including carbonate dissolution
47 and precipitation); and magmatic processes (e.g., underplating and volcanic loading).

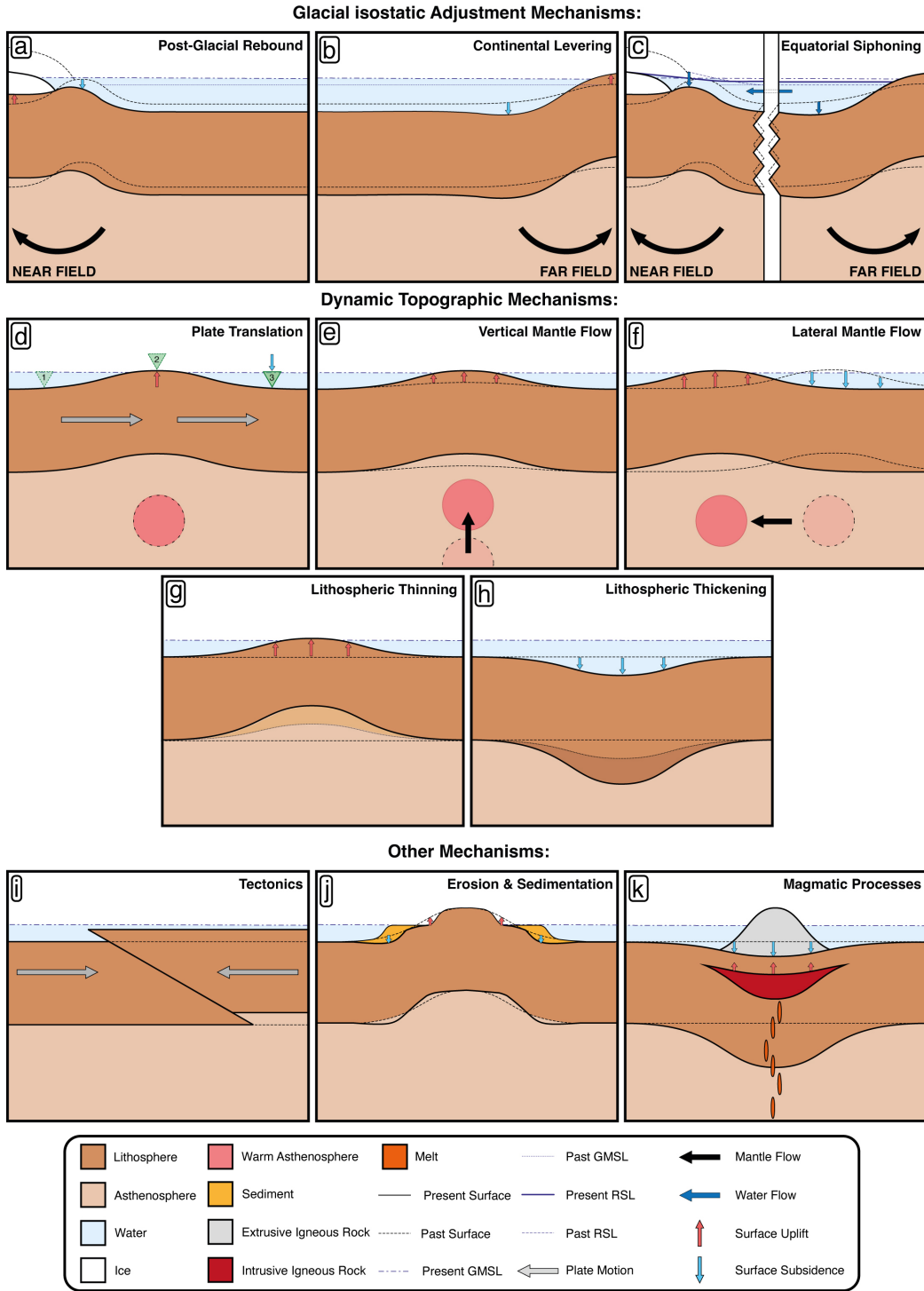


Figure 1: Processes affecting long-term RSL change. (a) Postglacial rebound. Surface uplift beneath ice sheet following melting; subsidence in peripheral bulge region. (b) Continental levering. Surface uplift along continental margin following ice sheet melting; subsidence offshore. (c) Equatorial ocean siphoning. Water migration to subsiding regions following ice sheet melting (i.e., peripheral bulge and offshore continental margins) causes far-field RSL fall; reduced gravitational pull of ice sheet drives near-field RSL fall. (d) Plate translation. Green arrows mark locus of sea-level marker as a function of time. (e) Vertical mantle flow. (f) Lateral mantle flow. (g) Lithospheric thinning. (h) Lithospheric thickening. (i) Tectonics, including short-term pre-/co-/post-seismic deformation and long-term crustal thickening/thinning. (j) Erosion and sedimentation, including carbonate dissolution/precipitation. (k) Magmatic processes, including surface subsidence from volcanic loading/uplift from magmatic underplating.

48 2.1. *Glacial Isostatic Adjustment*

49 At periodic intervals over the past \sim 3 million years, Earth's polar ice sheets have expanded far
50 beyond their present footprint during *glacials*, particularly in the Northern Hemisphere where large
51 fractions of the North American and Eurasian continents have been covered by kilometre-thick ice
52 masses, termed the Laurentide and Fennoscandian ice sheets, respectively (Raymo, 1994). These
53 glacials have been punctuated by *interglacial* periods, in which ice sheets rapidly collapsed back to
54 a configuration similar to their present extent. During these glacial-interglacial cycles, exchange of
55 water between ice and ocean reservoirs has been sufficient to raise and lower global mean sea-levels
56 by \sim 100 m. These huge mass transfers trigger deflections of both the Earth's solid surface and its
57 *geoid* (the gravitationally controlled equilibrium shape of the ocean surface) that are collectively
58 referred to as *glacial isostatic adjustment* (GIA).

59 Since the solid Earth deforms like a viscoelastic material, the GIA signal associated with the
60 growth and decay of ice sheets comprises both an elastic component, which responds instanta-
61 neously to changing ocean and ice loads, and a viscous component, which exhibits time-dependent
62 behaviour. The latter contribution, coupled with high mantle viscosities, explains why the crust
63 is still rebounding in areas previously covered by the Laurentide and Fennoscandian ice sheets,
64 despite their collapse ending over 7 thousand years ago. This *postglacial rebound* or *glacioisostasy*
65 is manifest in the ongoing sea-level fall of \sim 10 mm yr $^{-1}$ in parts of Hudson Bay and the Gulf of
66 Bothnia (Figure 1a; Bungum and Eldholm, 2022). Similarly, faster-than-average sea-level rise in
67 regions such as Chesapeake Bay, results from subsidence of the peripheral bulge surrounding the
68 former ice sheets.

69 Glacioisostatic surface deflections dominate the signal of GIA-induced RSL change in *near-*
70 *field* regions close to ice sheet margins. However, in *far-field* locations remote from ice sheets,
71 geoid and surface perturbations associated with shifting ocean loads, collectively referred to as
72 *hydroisostasy*, are most prominent. One key hydroisostatic mechanism is *continental levering*,
73 whereby water loading of previously air-loaded margins during deglaciation induces \sim 0.5 mm yr $^{-1}$
74 subsidence offshore and up to \sim 1 mm yr $^{-1}$ uplift onshore (Figure 1b; Mitrovica and Milne, 2002).
75 The increase in ocean basin volume that ensues, combined with that caused by peripheral bulge
76 collapse in the near-field, draws water away from equatorial regions, resulting in \sim 0.5 mm yr $^{-1}$
77 sea-level fall at low-latitude ocean islands in a second hydroisostatic process known as *equatorial*
78 *ocean siphoning* (Figure 1c).

79 Variations in glacial loading also perturb Earth's inertia tensor, modifying the orientation of the
80 solid Earth with respect to its spin axis. The shift in the position of the equatorial bulge caused by
81 this *true polar wander* creates a long-wavelength (\sim 15,000 km) pattern of relative uplift in regions
82 that move closer to the new equator and subsidence elsewhere. This mechanism is responsible for
83 the progressive shift of Earth's rotation axis towards Hudson Bay since the Last Glacial Maximum
84 (LGM; 27 ka). Although the impact of this rotational feedback on RSL is relatively small (10^1 – 10^2
85 times less than that due to glacioisostasy), it is a non-negligible contributor to far-field patterns
86 (Mitrovica et al., 2005).

87 The GIA-induced RSL changes described above mostly result from the displacement of Earth's
88 solid surface. However, the evolution of Earth's gravitational field during glacial cycles also sig-
89 nificantly alters spatial patterns of RSL change through both the instantaneous *direct effect* of
90 ice-sheet-to-ocean mass flux and the slower evolving *indirect effect* arising from solid Earth re-
91 sponses to this mass transfer. For example, the direct effect of melting the Greenland Ice Sheet
92 would manifest in a nearly instantaneous sea-level fall in Scotland and other near-field sites (e.g.,
93 Northern Labrador) because ocean surface lowering caused by the ice sheet's reduced gravitational
94 pull would locally overwhelm the effect of adding water to the global ocean (Kopp et al., 2015).

95 By contrast, the indirect effect of this melting would be apparent in local increases in the ocean
96 surface height resulting from mass flux of solid Earth material into the region previously depressed
97 by the former ice load.

98 Note that, in addition to affecting patterns of relative sea-level change, GIA impacts the re-
99 lationship between palaeo-ice volume and GMSL by altering the geometry of ocean basins. For
100 example, it is estimated that complete collapse of the Greenland and West Antarctic ice sheets
101 would drive sufficient surface rebound in these regions to eventually (after $\sim 10^4$ years) reduce
102 ocean basin volume by an amount equivalent to 2 m of GMSL. The total increase in GMSL result-
103 ing from this ice-to-water mass transfer would therefore be 14 m rather than the 12 m expected if
104 a fixed, present-day ocean basin geometry were assumed (Raymo et al., 2011).

105 During post-Pliocene ice age cycles GIA processes have acted in concert to generate $\sim 10^0 -$
106 10^2 m deviations in local sea-level from contemporary GMSL (Horton et al., 2018). Although this
107 signal is more muted in regions remote from the evolving land-based ice masses, its ubiquity means
108 that, even at far-field sites, geomorphic palaeo-sea-level records must be carefully corrected when
109 estimating palaeo-GMSL and ice volume (Figure 2). An added complication is that, while viscosity
110 might locally be low enough to produce centennial or decadal relaxation times, on a global scale,
111 relaxation times are typically multimillennial (Barletta et al., 2018). This long timescale means
112 that the solid Earth system has never fully reached isostatic equilibrium during any post-Pliocene
113 glacial cycle. Recovery from preceding ice and ocean load changes has therefore been continuously
114 interrupted and overprinted by the onset of the next cycle. These complexities make detailed
115 knowledge of mantle viscosity and ice sheet history a prerequisite for determining palaeo-GMSL
116 variations from geomorphic RSL markers.

117 2.2. Mantle Dynamic Topography

118 Although most of Earth's topography is *isostatic* (i.e., controlled by variations in the thick-
119 ness and density of the crust and lithosphere), stresses exerted on the base of the lithosphere by
120 convective flow within the underlying mantle can also generate km-scale topographic variations
121 (Hoggard et al., 2021). This so-called mantle *dynamic topography* is ubiquitous and continuously
122 evolves along with the planform of convection, causing vertical deflections of Earth's solid surface
123 that vary substantially as a function of space and time. These mantle-driven vertical motions
124 were originally thought to evolve slowly (< 5 m Myr $^{-1}$; e.g., Müller et al., 2008) and therefore
125 to have negligible impact on LIG ($\sim 129 - 116$ ka) palaeoshoreline elevations and limited influence
126 on MPWP ($\sim 3.3 - 3.0$ Ma) counterparts. However, recent studies have inferred rates of ~ 100 m
127 Myr $^{-1}$, suggesting that dynamic topography is an important consideration for palaeoshoreline-
128 based inferences of GMSL during all warm periods pre-dating the Holocene (Figure 2; Hoggard
129 et al., 2021)

130 Spatio-temporal changes in dynamic topography can be generated via a range of end-member
131 mechanisms including plate translation over a fixed convective planform (Figure 1d), vertical and
132 lateral convective flow of internal density anomalies (Figure 1e-f), and changes in lithospheric
133 thickness (Figure 1g-h). Several of these processes may be acting simultaneously in a given geo-
134 dynamic context. For example, upwelling of hot mantle material will often drive lithospheric
135 reheating and thinning, with the total reduction in lithospheric thickness potentially depending
136 on the rate of plate translation over this convective planform. Consequently, it is often difficult to
137 accurately quantify these different contributions to overall dynamic topography change.

138 In addition to inducing spatially variable RSL changes, dynamic topography may affect GMSL
139 directly, for example by generating net uplift over ocean basins (e.g., ~ 1 m Myr $^{-1}$ Conrad and

140 Husson, 2009), or by altering equilibrium ice sheet thickness through deflection of subglacial topog-
141 raphy. For example, an additional contribution to MPWP sea-level of 1–3 m has been attributed
142 to relative depression of Wilkes Basin topography during this period (Austermann et al., 2015).

143 2.3. Tectonics

144 Steady accumulation of fault-related vertical land motions can cause significant RSL change
145 over the timescales relevant to Plio-Pleistocene GMSL reconstruction (Figure 1i). The rate of this
146 tectonic uplift and subsidence varies widely from location to location, with stable cratonic regions
147 (e.g., western Australia, Scandinavia and central North America) inferred to have experienced
148 negligible tectonic activity ($\leq 0.01 \text{ mm yr}^{-1}$; e.g., Burbidge et al., 2009), while convergent plate
149 margins record rates of 1–10 mm yr^{-1} (e.g., Papua New Guinea, and the Alaskan and British
150 Columbian stretches of the Pacific Coast Ranges; Pfeffer et al., 2017; Figure 2). Correcting for
151 these perturbations is complicated by the fact that many long-term uplift and subsidence estimates
152 are derived from thermochronological data with low spatio-temporal resolution, potentially aliasing
153 short-timescale tectonic RSL changes at certain sites. Nevertheless, high uplift rates can promote
154 the formation and preservation of flights of marine terraces from multiple sea-level highstands.
155 Vertical separation between these terraces may therefore allow relative GMSL variation within
156 individual glacial cycles to be deduced, provided uplift rates can be independently constrained and
157 assumed to be relatively constant on these 10^4 -year timescales (Malatesta et al., 2022).

158 On long timescales, rifting of passive margins, continental collision, and changes in mid-ocean
159 ridge spreading rate can drive significant GMSL variation by modifying the total volume of ocean
160 basins (Wright et al., 2020). There is some controversy regarding the true magnitude of these
161 GMSL variations. For example, it has been argued that age-dependent subsidence of the cooling
162 oceanic lithosphere should be included in the definition of dynamic topography (Forte and Rowley,
163 2022). In this formalism, changes in spreading rate and the average age of oceanic lithosphere
164 would constitute a shift in oceanic mantle dynamic topography that must be compensated by an
165 opposing shift in continental regions, since the global integral of this field should be equal to zero.
166 If confirmed, this compensation mechanism would imply that many long-term sea-level estimates
167 are inaccurate because they assume that continental hypsometry is time-invariant. However, a
168 recent numerical modelling study that simultaneously accounts for changes in oceanic and conti-
169 nental topography finds that increased mid-ocean ridge spreading rate tends to correlate with more
170 negative continental dynamic topography, the opposite trend to that expected if such compen-
171 sation were in operation (Young et al., 2022). Clearly, further work is needed to clarify this matter,
172 but whatever the outcome of the debate, the total amplitude of tectonic GMSL change is not
173 thought to have exceeded $\sim 1 \text{ m Myr}^{-1}$ in the past 5 Myrs, although revised plate reconstructions
174 do suggest a global slowdown in spreading rate that may have generated more pronounced GMSL
175 reduction between 15 and 5 Ma (Dalton et al., 2022).

176 2.4. Erosion and Sedimentation

177 Transfer of rock mass via erosion and sedimentation, or precipitation and dissolution, alters the
178 position and amplitude of surface loads applied to the crust. This shift in loading pattern perturbs
179 both the geoid and Earth’s solid surface and can therefore lead to significant RSL change ($\sim 0.05\text{--}$
180 0.5 mm yr^{-1}) in mountainous areas and coastal regions that are subject to karstification or close
181 to major sedimentary depocentres (e.g., deltas and coral reefs; Creveling et al., 2019; Pico, 2020;
182 Figure 1j). In addition, unconsolidated sediment will compact under its own weight, expelling
183 water from its pore space into the global ocean and potentially lowering solid surface elevations
184 by up to 5 mm yr^{-1} along coastal plains and deltas (Figure 2). Observational constraints on past

185 sediment flux are therefore essential for inferring palaeo-GMSL from RSL markers deposited on
186 top of poorly consolidated sediment or at sites proximal to major deltas or reefs. The viscoelastic
187 properties of the lithosphere around these depocentres must also be estimated, since they control
188 the amplitude and wavelength of sedimentation-related uplift and subsidence (Watts, 2001).

189 GMSL can also be affected by sedimentation patterns. For example, increased sediment de-
190 position and carbonate precipitation will displace water, leading to sea-level rise. Although such
191 variations in the global sediment budget are partially compensated by loading-induced crustal de-
192 flexions, they can have a non-negligible impact on long-term GMSL trends ($\sim 0.5 \text{ m Myr}^{-1}$; Young
193 et al., 2022).

194 2.5. Magmatic Processes

195 The impact of magmatic processes on long-term RSL changes is most apparent at ocean islands.
196 Progressive growth of their volcanic edifices load the crust, driving subsidence of fringing RSL
197 markers at rates of up to $\sim 5 \text{ mm yr}^{-1}$ (Huppert et al., 2015; Figure 1k). At the same time, crustal
198 thickening via underplating of intrusive material close to the crust-mantle boundary can drive
199 countervailing isostatic uplift of ocean islands, albeit at slower rates ($\sim 0.05 \text{ mm yr}^{-1}$; Ramalho
200 et al., 2017; Figure 2). An additional consideration when assessing magmatic impacts is that even
201 after volcanic activity has ceased on one island, RSL indicators can be perturbed by the ongoing
202 growth of adjacent loads, as is commonly the case in ocean island chains created by plate motion
203 over a relatively stationary mantle plume (Huppert et al., 2015). These substantial changes in
204 land elevation inevitably complicate efforts to constrain GMSL on ocean islands that are either
205 volcanically active or else located close to sites of active magmatism.

206 Changes in the rate of magmatic addition to the crust and lithosphere also affect ocean basin
207 volume, modulating GMSL on long timescales. In particular, eruptions of submarine *Large Igneous*
208 *Provinces* (e.g., the Ontong-Java Plateau) can potentially cause punctuated metre-scale increases
209 in GMSL. Nevertheless, despite a significant contribution to the sea-level budget ($\sim 20\text{--}50 \text{ m GM-$
210 SLE; (Wright et al., 2020; Young et al., 2021)), available evidence suggests that, on $10^0\text{--}10^1 \text{ Myr}$
211 timescales, submarine eruption rates and their impact on sea-level have varied minimally since 200
212 Ma ($\sim 0.1 \text{ m Myr}^{-1}$).

213 3. Quantifying GMSL Variations from Geomorphic Proxies

214 Geomorphic records of palaeo-sea level variation are invariably affected by some combination of
215 the post-depositional processes detailed above. Inferring GMSL variation from these observations
216 therefore requires analysis to be restricted to regions where each of these perturbations can either
217 be accurately quantified, or else assumed to have negligible impact. Unfortunately, no site on
218 Earth preserves a pristine record of palaeo-sea-level change since two of these processes—GIA and
219 dynamic topography—are ubiquitous and must therefore be constrained. At sites remote from
220 major ice sheets, incomplete knowledge of mantle rheology and past ice configuration translates
221 into relatively minor uncertainty in GIA-induced RSL change, allowing useful inferences of palaeo-
222 GMSL to be drawn from geomorphic records in the far-field. However, the impact of uncertain
223 mantle structure on dynamic topography is of comparable magnitude everywhere on Earth’s surface
224 and must be accounted for at all localities when inferring pre-Holocene sea-level.

225 The relationship between different sea-level proxies (e.g., salt marsh sediments, fossil reefs,
226 beach deposits, marine terraces, and archaeological records) and time-integrated mean sea-level,
227 also known as the *indicative range* of a sea-level indicator, introduces further uncertainty into
228 GMSL inferences. For example, the elevation above mean sea level of a beach ridge strongly

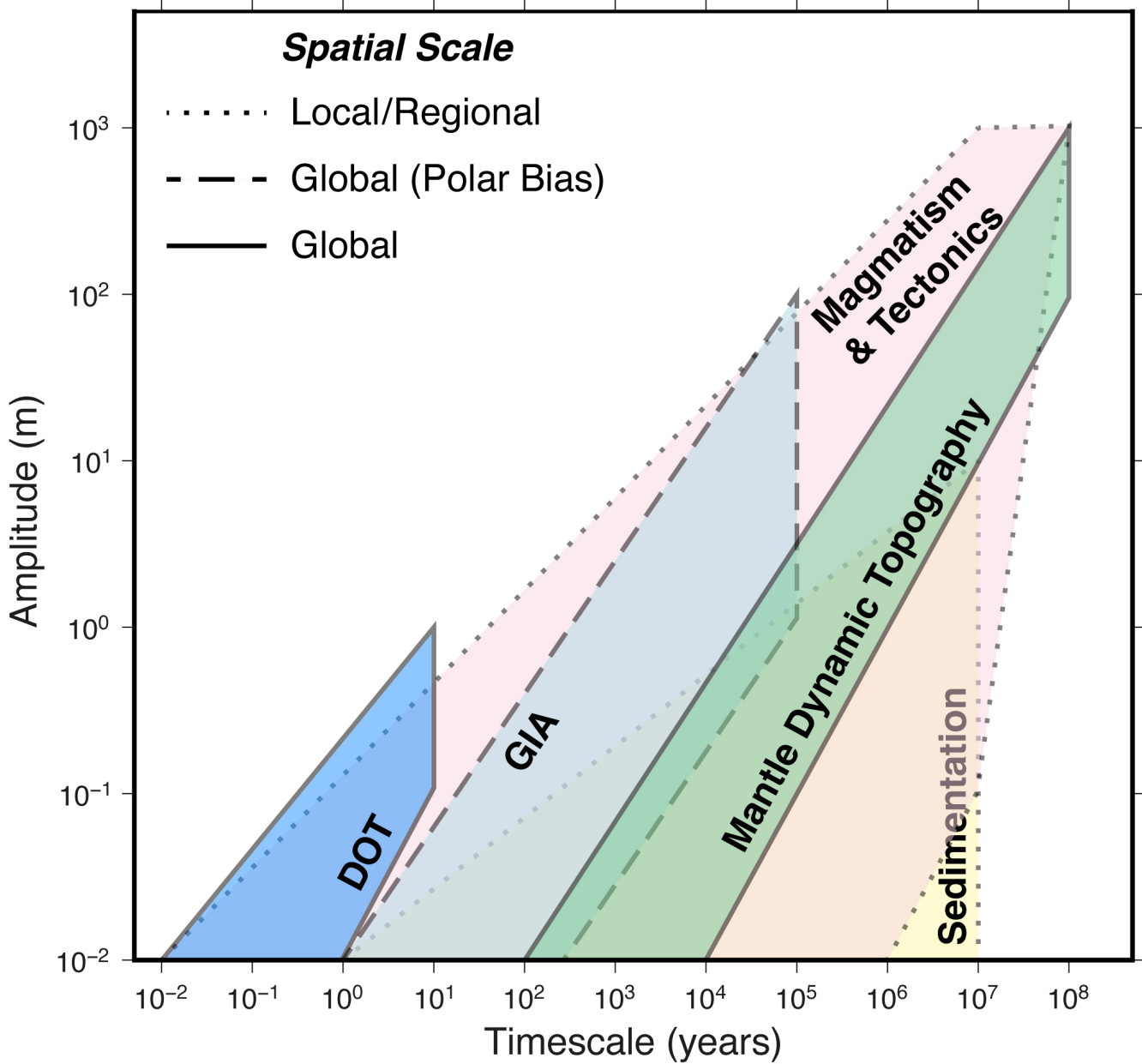


Figure 2: Characteristic duration and magnitude of processes affecting RSL variation. DOT = Dynamic Ocean Topography. Note that although magmatism, tectonics and sedimentation can generate > 10 m RSL change on long timescales, their influence is localised.

depends on local wave energy (1–6 m), while corals often have wide habitat depth distributions (~ 10 m–0 m) that vary by species Hibbert et al. (2016). The precision to which these different markers can be dated varies according to the analytical technique used, which depends in turn upon their composition, preservation, and overall age (e.g., radiocarbon dating is typically more precise than U-Th dating, but is only feasible for sea-level indicators less than $\sim 50,000$ years old; Murray-Wallace and Woodroffe, 2014). Age uncertainties can therefore become large compared with the length of a target interglacial or warm period, especially for older sea-level indicators.

Despite these uncertainties associated with geodynamic processes, palaeo-water depth, and age of formation, geomorphic sea-level indicators can generally constrain interglacial GMSL better

than isotopic records. The mid-Pliocene Warm Period and Last Interglacial have been of particular interest, since climate during these periods was sufficiently similar to that of the present-day and expected near-future that studying their sea-level histories may help to predict changes over the coming centuries. Our understanding of sea-level during these periods is therefore the focus of the following section; however, other key Plio-Pleistocene warm periods are summarised to add context.

3.1. Mid-Pliocene Warm Period

The Mid-Pliocene Warm Period (MPWP), 3.0–3.3 million years ago, represents the most recent time in Earth history that atmospheric CO₂ concentrations and global mean temperatures reached values approaching those expected over the course of the next century (~340–460 ppm and ~2–3°C above pre-industrial; Rae et al., 2021). Consequently, estimates of global mean sea level (GMSL) during this period are valuable for ongoing efforts to determine future ice sheet stability in the face of prolonged warming.

Determining MPWP palaeo-ice volume from geomorphic proxies is complicated by the potential for convectively driven ~10¹–10² m surface deflections to have accrued over the 3 million years that have elapsed since this time interval. Although inferences of palaeo-ice volume from isotopic datasets partly circumvent this issue, MPWP GMSL estimates derived in this way range from 6–58 m above present day values (Grant and Naish, 2021). Provided post-depositional effects can be reliably constrained and corrected for, geomorphic proxies are therefore more likely to yield accurate and precise GMSL constraints. Indeed, the range of published values derived from geomorphic data is narrower than the geochemically inferred equivalent (+6–35 m versus +6–58 m), despite including estimates that make no attempt to correct for dynamic topography (Grant and Naish, 2021).

The amplitude of glacial-to-interglacial GMSL change during the MPWP can be determined relatively reliably at far-field sites because slow-evolving dynamic topographic perturbations can be separated from the shorter period (~10⁴-year) glacioeustatic cycles. For example, high-resolution sedimentary records from the Whanganui Basin in New Zealand indicate a difference in GMSL between MPWP glacials and interglacials of between 6 and 17 m (16th and 84th percentiles; Grant and Naish, 2021). However, such records are unable to constrain absolute values of MPWP GMSL compared to the present-day without independent knowledge of ice sheet configuration during at least one of these mid-Pliocene intervals.

Absolute GMSL can be obtained in locations where a sufficiently long and continuous record of relative sea-level change is available. In such cases, mantle-driven uplift or subsidence can be estimated by comparing the vertical separation between sea-level markers formed during different warm periods to expected relative GMSL differences derived from independent reconstructions. This approach has been applied to 3.1–4.8 Ma relative sea-level variations recorded by phreatic overgrowths in Mallorcan caves, yielding long-term uplift rates of 0.6–4.4 m Myr⁻¹ and corrected MPWP GMSL of +6.8–20.4 m (including +1.2 m thermosteric contribution; Dumitru et al., 2019).

An alternative strategy, made possible by recent improvements in our understanding of Earth's three-dimensional density and viscosity structure, is to constrain dynamic topography directly using simulations of mantle convection. For example, an MPWP GMSL of ~15 m has been inferred by correcting the elevation of the ~800 km-long Orangeburg Scarp palaeoshoreline (Eastern USA) for predicted post-depositional deflections due to dynamic topography, as well as GIA and flexural deformation arising from erosion and sedimentation (Moucha and Ruetenik, 2017). However, the limited range of convection simulations typically applied in such studies, and their restriction to single localities, makes it difficult to quantify the impact of uncertain mantle structure and

evolution on the final GMSL estimate. Moreover, in the specific case of the Orangeburg Scarp, GIA and sediment loading are also important factors due to its proximity to the former Laurentide Ice Sheet and substantial post-Pliocene sediment deposition offshore, each translating into potentially significant but poorly quantified GMSL uncertainties.

Many of these limitations can now be addressed through methodological refinements. First, *emulators* (i.e., computationally efficient approximators) can be trained on ensembles of mantle convection and GIA simulations that provide acceptable fit to geodynamic observables. Once appropriately calibrated, these emulators can rapidly post-depositional deflections for a broad range of uncertain Earth model parameters. By integrating these functions into a probabilistic inverse framework it is then possible to robustly propagate uncertainties in solid Earth structure into MPWP GMSL estimates. Secondly, by simultaneously correcting geomorphic RSL data from multiple sites, a more globally representative GMSL value can be obtained, while also improving constraint on Earth's internal structure based on which density and viscosity inputs best reconcile the vertical offset between sea-level markers at different sites. Finally, by concentrating on regions remote from major ice sheets with minimal tectonic activity and slow rates of erosion and sedimentation, uncertainty associated with post-depositional processes can be minimised, increasing the precision of GMSL estimates. A recent application of this approach to a suite of continent-wide offshore and onshore RSL constraints around Australia yields an MPWP sea-level estimate of $+16.0^{+5.5}_{-5.6}$ m (Richards et al., 2022; Figure 3).

Although efforts to correct MPWP sea-level markers for dynamic topographic perturbations remain at an early stage, estimates that do correct for this long-term uplift and subsidence suggest that GMSL was at least 7 m above present, but reached no higher than +21 m (Moucha and Ruetenik, 2017; Dumitru et al., 2019; Hearty et al., 2020; Richards et al., 2022). After accounting for an inferred thermosteric contribution of ~ 1.2 m, this range suggests that the Greenland (7 m GMSL equivalent; GMSLE) and West Antarctic (~ 5 m GMSLE) Ice Sheets were both smaller during the Mid-Pliocene, with loss of marine-based sectors of the East Antarctic Ice Sheet also possible in the case of high-end GMSL values. Note, however, that the relative contribution of these different ice sheets—and the degree to which they are in or out of phase with one another—is mainly inferred from numerical modelling studies (e.g., de Boer et al., 2017), since available observational evidence (e.g., ice-raftered debris records and cosmogenic nuclide exposure ages) has coarse spatiotemporal resolution (e.g., Bierman et al., 2016).

3.2. Last Interglacial

The Last Interglacial period (LIG), also referred to as the Eemian or Marine Isotope Stage 5e (MIS 5e), lasted approximately 13 thousand years from ~ 129 to 116 thousand years before present. Although atmospheric CO₂ concentrations are estimated to have been significantly lower than present-day values (265–285 ppm; comparable to the pre-industrial era), globally averaged temperatures are thought to have been the same or higher (i.e., $\sim 1^{\circ}\text{C}$ above pre-industrial levels; Rae et al., 2021). Moreover, due to higher orbital eccentricity during this period, polar temperatures are thought to have been significantly higher than present, with Greenland and Antarctica reaching 5–8°C and 3–5°C above pre-industrial temperatures, respectively (e.g., Landais et al., 2016). GMSL estimates for this period therefore represent a useful constraint on equilibrium ice volumes during periods of prolonged warmth, even if LIG orbital forcing differs from that of the modern era.

Having previously been assumed to be negligible, a consensus is emerging that dynamic topographic perturbations to LIG sea-level markers can reach up to $\sim \pm 10$ m (e.g., Austermann et al., 2017). While significantly smaller than Pliocene-to-Recent deflections, these vertical land

330 motions are of comparable magnitude to the total estimated GMSL difference between the LIG
331 and the present, and must therefore be carefully considered when interpreting RSL markers from
332 this period. GIA-induced RSL variation during the LIG is also of similar amplitude, albeit with a
333 distinct spatial pattern that is, at least theoretically, feasible to separate from dynamic topography
334 change.

335 Traditional estimates of LIG GMSL from geomorphic proxies generally correct for GIA-related
336 sea-level change, but assume an Earth viscosity structure that varies only radially. Resulting
337 values of peak LIG GMSL range between 4 and 9 m above present depending on the site of the
338 corrected sea-level markers (Dutton et al., 2015; Dyer et al., 2021). A portion of this inter-site
339 discrepancy has been resolved in certain regions by accounting for three dimensional variations
340 in viscosity (e.g., Austermann et al., 2021). For example, studies using radial viscosity models
341 in their GIA calculations, infer an early LIG GMSL peak of 7.6 ± 1.7 m from sea-level indicators
342 in the Seychelles, whereas contemporaneous estimates from Western Australia yield an estimate
343 of $\sim 3.4 \pm 0.6$ m (Dutton and Lambeck, 2012). This ~ 4 m discrepancy can be reduced to ~ 2 m
344 by accounting for lateral variations in viscosity and lithospheric thickness in calculations of GIA-
345 induced RSL change (Austermann et al., 2021). The remaining ~ 2 m mismatch could result from
346 variations in LIG-to-present dynamic topography change between the sites (Austermann et al.,
347 2017); however, further work is required to conclusively validate this hypothesis.

348 A key complication associated with inferring LIG GMSL is the large uncertainties in the two
349 main parameters that control GIA: ice history and mantle viscosity. Even at far-field sites, the
350 wide range of plausible GIA model inputs propagates into GMSL uncertainties of several metres
351 when each ice history-viscosity pair in a given model ensemble is assumed to be equally likely.
352 To address this issue, Dyer et al. (2021) recently developed a Bayesian inverse framework that
353 weights individual predictions of GIA-induced RSL change from a ~ 600 model ensemble based on
354 their ability to accurately reproduce observed spatiotemporal trends in Bahamian LIG sea-level
355 indicators (Figure 4a–m). This approach also enables data with highly variable age and water depth
356 uncertainties to be incorporated in a statistically robust manner. Significantly, the resulting GMSL
357 estimate of 1.7–4.6 m (16th–84th percentiles) is significantly lower than most previous estimates and
358 outside the ‘likely’ range of the IPCC AR6 report (5–10 m; Fox-Kemper et al., 2021; Figure 4n–
359 o). If this result is replicated elsewhere, it would imply that polar ice sheets are less sensitive to
360 high-latitude warming than currently thought. Alternatively, if responses of the Greenland and
361 Antarctic Ice Sheets to warming were antiphased, elevated ice sheet sensitivity would remain a
362 possibility.

363 The timing of peak GMSL within the LIG is controversial with different studies arguing for
364 an early peak, a late peak, and even multiple peaks due to orbitally driven asynchronicity in
365 ice loss from the Antarctic and Greenland Ice Sheets (Horton et al., 2018). Ice-sheet modelling
366 and ice core-based reconstructions are beginning to reach consensus on a 0.5–3.5 m LIG sea-level
367 contribution from the Greenland Ice Sheet (e.g., Plach et al., 2019), while an additional ~ 1 m
368 is expected due thermal expansion and melting of mountain glaciers (Rohling et al., 2019). The
369 Antarctic contribution to LIG GMSL remains unclear, since large uncertainties in peak LIG GMSL
370 combined with a lack of direct evidence for contemporaneous mass loss permit values anywhere
371 between 0 and 6 m GMSL.

372 3.3. Other Plio-Pleistocene Warm Periods

373 3.3.1. Pliocene Climatic Optimum

374 The Pliocene Climatic Optimum (PCO; ~ 4.4 –4.0 Ma) was the warmest interval in the last 5
375 million years, with global mean temperatures approximately 4°C higher than pre-industrial values

and elevated atmospheric CO₂ (~400–470 ppm; Rae et al., 2021). Geomorphic sea-level indicators from this period are sparse, complicating assessment of GMSL. However, records from Mallorca and Argentina that have been locally corrected for long-term uplift and GIA indicate 11–28 m (Dumitru et al., 2019; Hollyday et al.), broadly consistent with ice-sheet modelling studies that suggest ~8.5 m and ~7 m GMSLE contributions from Antarctica and Greenland, respectively, with an additional ~1.5 m from thermosteric effects (Golledge et al., 2017). A >4 m Antarctic contribution is compatible with independent evidence from offshore sedimentary records, which suggest significant early Pliocene ice loss in the Wilkes Subglacial Basin of East Antarctica (Bertram et al., 2018). Similarly, the limited volume of ice rafted debris recorded offshore Greenland implies only small, ephemeral ice sheets were present during this interval (Bailey et al., 2013). Consensus therefore appears to be building that the PCO was characterised by lower ice volume and higher GMSL than the MPWP, consistent with its more elevated CO₂ and temperature levels. It may therefore provide a useful guide to future sea-level trajectories in the event that atmospheric CO₂ remains significantly above 400 ppm throughout the coming centuries.

3.3.2. MIS 11

MIS 11 (~420–370 ka) was a peculiarly long interglacial and details of the climatic conditions during this period remain somewhat enigmatic. Global mean temperature estimates range from 1–2°C above preindustrial levels and atmospheric CO₂ concentrations appear to have been similar to other Quaternary interglacials (~280 ppm; Rae et al., 2021). However, sea-level reconstructions that have been corrected for tectonic deformation and GIA indicate a remarkably large reduction in polar ice volumes (6–13 m GMSLE) during this period, an inference corroborated by independent geochemical and palaeobiological data sets that point to substantial retreat of both the Antarctic and Greenland ice sheets (Roberts et al., 2012; Raymo and Mitrovica, 2012; Tzedakis et al., 2022). The unusually protracted duration of this interglacial was likely key to triggering such widespread ice loss, and has been linked to antiphasing of obliquity and precession cycles (Tzedakis et al., 2022). These relatively unique features complicate direct comparisons of MIS 11 with ongoing climatic changes.

MIS 11 palaeoshorelines from relatively tectonically stable regions are restricted to single sites in the Bahamas, Bermuda, eastern USA, southeastern Australia and South Africa. This sparse spatial distribution hinders efforts to deconvolve RSL changes induced by GIA and dynamic topography from GMSL variations during this period, leading to deep uncertainty in existing sea-level estimates. An additional issue is that ice histories are not well constrained in the lead-up to MIS 11, limiting the precision and accuracy of GIA predictions across this interval (Tzedakis et al., 2022). Nevertheless, the balance of current evidence, suggests that MIS 11 GMSL had a higher peak than the LIG, with substantial loss of ice from southern Greenland and the Wilkes Basin in East Antarctica.

3.3.3. Mid-Holocene Warm Period

Proxy records suggest the Mid-Holocene Warm Period (~8–3 ka) was characterised by marginally lower global mean temperature (~0.75°C above preindustrial levels) and atmospheric CO₂ (260–270 ppm) than the LIG, although Northern Hemisphere temperatures may have reached ~4°C above preindustrial levels (Dutton et al., 2015; Rae et al., 2021). However, the proposed long-term cooling trend following this early peak is at odds with climate simulations that point to progressive warming over the same time interval (Horton et al., 2018). This discrepancy is yet to be resolved, confounding efforts to understand the mechanisms driving climatic changes throughout this period. Nevertheless, sea-level evolution over the same period is relatively well constrained thanks to an

abundance of preserved coastal deposits and the applicability of high-resolution dating techniques. In addition, the recency of this warm period minimises pollution of the GMSL signal with dynamic topography and enables accurate reconstruction of past ice extent (at least in the Northern Hemisphere), allowing spatial variations in RSL to be more confidently tied to GIA processes.

Far-field GMSL estimates during this period obtain a peak of 1–6 m (Horton et al., 2018). Much of this apparent highstand is attributed to equatorial ocean siphoning; however, some evidence exists for a less extensive West Antarctic Ice Sheet at this time (Kingslake et al., 2018). If readvance of this ice sheet following the Mid-Holocene is proven, it would underline how local GIA-induced changes in bedrock elevation can interact with global scale sea-level changes, partially decoupling GMSL variation from direct climatic changes. Despite this uncertainty mid-Holocene Antarctic ice volumes, this period provides important constraints on the typical rate of interglacial sea-level change resulting from natural climate variability, allowing the recent acceleration in GMSL rise to be confidently attributed to anthropogenic impacts.

3.4. Synthesis

Increasingly accurate correction of relative sea-level data for post-depositional geodynamic perturbations is yielding new insight into ice volumes during past warm periods. These analyses generally reduce inferred palaeo-GMSL for key warm periods, bringing them into better agreement with predictions from ice-sheet modelling studies. It therefore appears, perhaps unsurprisingly, that a significant fraction of the pre-existing discrepancy resulted from a bias in the palaeoshoreline record towards regions experiencing long-term relative sea-level fall.

The revised palaeo-GMSL estimates correlate strongly with contemporaneous global mean temperature reconstructions, although this relationship is clearly non-linear (Figure 5). An additional complication is that the timescale over which warming is sustained may exert a strong control on palaeo-ice volume (e.g., compare sea-levels during MIS 5e and MIS 11). Overall, constraint on peak GMSL during key warm periods has improved significantly in the past decade. However, determining the relative contribution of Greenland, West Antarctica, and East Antarctica to past sea-level change remains challenging due to the current sparsity of palaeoshoreline data and direct constraints on former ice extents. In addition, it is unclear how mantle flow-driven changes in bed elevations may have altered the equilibrium grounded ice capacity of these ice sheets through time. Resolving these issues is crucial for ongoing efforts to better integrate palaeo sea-level constraints into future sea-level projections.

4. Outlook: Refining Sea-Level Reconstructions with New Datasets and Geodynamic Modelling Techniques

Significant improvements in intermediate and long-term projections of future sea-level rise can be achieved if uncertainty on palaeo sea levels can be narrowed and revised estimates can be better integrated into modelling studies. Three key challenges currently impede efforts to increase precision and accuracy of GMSL estimates during past warm periods. First, the sparsity of existing geomorphic sea-level constraints complicates the differentiation of GMSL changes from spatially variable RSL signals related to post-depositional geodynamic processes. Secondly, the accuracy with which these RSL changes can be constrained, especially those arising from GIA and dynamic topography, is limited by uncertain mantle viscosity and density structure. The following sections outline possible solutions to each of these challenges.

463 *4.1. Improving Palaeo-Sea Level Data Coverage*

464 Natural limits on the formation and preservation of palaeoshoreline deposits place an upper
465 bound on achievable data densities, which becomes more restrictive as the age of the targeted
466 sea-level highstand increases. Nevertheless, significant gaps in the Neogene sea-level record can
467 be filled by leveraging existing data compilations. For example, the PalaeoDB palaeobiological
468 database contains global information on the occurrence of shallow marine fauna that—despite
469 generally having larger uncertainties than data from more targeted field studies—allow GIA and
470 dynamic topography predictions to be groundtruthed (Fernandes and Roberts, 2021). Similarly,
471 the abundance of publicly available well and seismic reflection datasets is constantly increasing
472 thanks to data sharing agreements between governmental organisations (e.g., Geoscience Australia)
473 and the geoenergy industry, allowing backstripping techniques to be applied to a significant fraction
474 of the world’s continental margins. Although uncertainties associated with sediment compaction
475 diminish the precision of backstripped sea-level records, their relative temporal continuity allows
476 local RSL trends to be inferred with reasonable reliability. Finally, continental-scale hiatus maps,
477 derived from analysis of conformable and unconformable contacts between rocks from successive
478 geological series, are sufficiently spatially complete to provide useful validation of geodynamic
479 model predictions despite their coarse temporal resolution (Hayek et al., 2020).

480 Continuous improvements in dating and data acquisition techniques are constantly increasing
481 the spatio-temporal resolution of the global palaeo-sea level record. Community efforts to build new
482 sea-level databases with standardised entry formats represent a particularly important advance,
483 e.g., the WALIS (World Atlas of Last Interglacial Shorelines) project (Rovere et al., 2022). Machine
484 learning techniques are also showing significant promise as a tool for expanding data coverage, with
485 neural networks increasingly used to automate detection of shallow marine facies in satellite-derived
486 digital elevation models (e.g., Dyer et al., 2021). In addition, integration of GIA and dynamic
487 topography model predictions within probabilistic inverse frameworks can guide the sampling
488 strategy of new field campaigns by quantifying the extent to which additional data points in a
489 given region will reduce uncertainty sea-level reconstructions. Finally, innovative dating techniques,
490 such as multiple-isotope cosmogenic nuclide approaches, coupled with continued improvement in
491 the precision of long-established methods, will enable the identification of new Plio-Pleistocene
492 shorelines and improve age constraint on existing deposits.

493 *4.2. Improving Models of Post-Depositional Impacts*

494 In recent decades, our ability to numerically model the impact of GIA and dynamic topogra-
495 phy on RSL indicators has grown significantly. However, it has also become increasingly apparent
496 that more accurate constraints on the 3D variations in mantle viscosity and density that drive
497 these processes are urgently needed. Fortunately, a number of recent breakthroughs indicate
498 that meeting this requirement is possible, at least regionally. First, new data compilations that
499 constrain present-day dynamic topography—when combined with existing non-hydrostatic geoid
500 height anomaly and core-mantle boundary excess ellipticity measurements—have allowed Earth’s
501 internal density and viscosity structure to be quantified in greater detail (Lu et al., 2020; Richards
502 et al., 2023). Secondly, theoretical and computational advances in seismic tomography are enabling
503 higher resolution imaging of Earth’s internal structure. Improved constraint on velocity variations
504 within the lithosphere and asthenosphere are especially valuable since GIA and dynamic topog-
505 raphy signals are dominated by shallow mantle structure on Plio-Pleistocene timescales. Thirdly,
506 experimental constraints on the elastic and anelastic behaviour of rocks at seismic frequencies are
507 improving our ability to convert Earth’s present-day seismic velocity structure into the physical
508 quantities of interest for GIA and dynamic topography modelling (i.e., temperature, density and

509 viscosity; Austermann et al., 2021; Lau et al., 2021; Ivins et al., 2023. Finally, powerful adjoint-based inverse methods have been developed that enable reliable reconstruction of mantle flow
510 back through time ('retrodiction') and allow inferred three-dimensional viscosity structure to be
511 refined using RSL observations ('viscosity tomography'; Ghelichkhan and Bunge, 2018; Crawford
512 et al., 2018).

513 Despite these innovations, the computational expense of calculating time-dependent changes
514 in GIA and dynamic topography using Earth models that include three-dimensional variations in
515 physical properties is substantial. In addition, although constraint on present-day Earth struc-
516 ture has improved, significant uncertainty remains due to limits on tomographic resolution and
517 non-unique conversions between seismic velocity and key physical properties. Given these twin dif-
518 ficulties, accurately propagating uncertainties in Earth structure into GMSL estimates is currently
519 problematic. However, new techniques that enable rapid calculation of approximate solutions (e.g.,
520 statistical emulation and surrogate modelling) may partially resolve these problems by unlocking
521 the ability to integrate complex model calculations into a probabilistic inverse framework. Some
522 of these frameworks also allow the incorporation of data with very different age uncertainties and
523 palaeo-water depth ranges. These advances are critical, since improving the sea-level projections
524 of ice-sheet models will rely on robust assessments of palaeo-GMSL that rigorously account for all
525 these sources of uncertainty.

527 5. Synthesis

528 Over the past decades it has become increasingly clear that a broad range of geodynamic
529 phenomena can cause relative sea levels to deviate significantly from globally averaged values.
530 The characteristic timescales, wavelengths and spatial patterns of these sea-level perturbations
531 varies significantly depending on the underlying process. Mantle dynamic topography evolves
532 slowest ($\sim 0.1 \text{ mm yr}^{-1}$) but has a ubiquitous impact and can produce hundred-metre deflections
533 in a few million years. By contrast, tectonic activity can produce metre-scale elevation changes
534 on centennial timescales, but such extreme vertical displacement is largely confined to narrow
535 regions along convergent plate boundaries. This separation of scales, patterns, and magnitudes
536 suggests that, with sufficient data coverage and continued improvement in our understanding of
537 the solid Earth, RSL patterns associated with different mechanisms can be detected, quantified
538 and corrected for, at least locally.

539 Although post-depositional geodynamic processes undoubtedly complicate the assessment of
540 palaeo-GMSL, significant progress has been made thanks to new RSL data, improved constraint
541 on Earth's internal structure, and advances in geodynamic and probabilistic modelling. Consensus
542 is now building that GMSL during the Mid-Pliocene Warm Period did not exceed $\sim 22 \text{ m}$. This
543 upper bound suggests that, if the Greenland Ice Sheet was less extensive than at the present-day,
544 a significant fraction of East Antarctic marine-based ice remained during this period. Similarly,
545 recent correction of Last Interglacial sea-levels for mantle dynamic topography and GIA produces
546 an upper limit (84th percentile) on peak GMSL of $\sim 4 \text{ m}$, lower than many previous estimates
547 (6–9 m). If confirmed, these reductions imply that some existing ice-sheet-model-based sea-level
548 projections may need to be revised downward as they are calibrated against LIG and MPWP
549 GMSL bounds that are excessively high.

550 It is clear from Holocene records that present rates of sea-level change are significantly more
551 rapid than at any other time during the present interglacial. However, longer term trajectories
552 remain unclear due, in large part, to remaining uncertainties in the palaeo sea-level record. Sig-
553 nificant progress can be made by increasing data coverage during poorly sampled intervals (e.g.,

the Pliocene Climatic Optimum and MIS 11), as well as corroborating recent low-end MPWP and LIG sea-level estimates in other regions. These goals are increasingly achievable thanks to recent improvements in data availability, advances in our knowledge of solid Earth structure and dynamics, and the development of Bayesian frameworks to rigorously propagate uncertainties in both geodynamic model parameters and input data into inferred GMSL histories. These probabilistic frameworks also allow the main sources of uncertainty to be identified, enabling field data collection and model refinement to be better targeted. Connecting palaeo sea-level variation to present and near-future trends will remain challenging due to inherent uncertainties and evolving climatic boundary conditions. Nevertheless, recent breakthroughs in palaeo sea-level reconstruction have enabled uncertainty in future projections to be both narrowed and robustly quantified in a manner that was previously infeasible.

References

- Austermann, J., Hoggard, M.J., Latychev, K., Richards, F.D., Mitrovica, J.X., 2021. The effect of lateral variations in Earth structure on Last Interglacial sea level. *Geophysical Journal International* 227, 1938–1960.
- Austermann, J., Mitrovica, J.X., Huybers, P., Rovere, A., 2017. Detection of a dynamic topography signal in last interglacial sea-level records. *Science Advances* 3.
- Austermann, J., Pollard, D., Mitrovica, J.X., Moucha, R., Forte, A.M., DeConto, R.M., Rowley, D.B., Raymo, M.E., 2015. The impact of dynamic topography change on Antarctic ice sheet stability during the mid-Pliocene warm period. *Geology* 43, 927–930.
- Bailey, I., Hole, G.M., Foster, G.L., Wilson, P.A., Storey, C.D., Trueman, C.N., Raymo, M.E., 2013. An alternative suggestion for the pliocene onset of major northern hemisphere glaciation based on the geochemical provenance of north atlantic ocean ice-raftered debris. *Quaternary Science Reviews* 75, 181–194.
- Barletta, V.R., Bevis, M., Smith, B.E., Wilson, T., Brown, A., Bordoni, A., Willis, M., Khan, S.A., Rovira-Navarro, M., Dalziel, I., et al., 2018. Observed rapid bedrock uplift in amundsen sea embayment promotes ice-sheet stability. *Science* 360, 1335–1339.
- Bertram, R.A., Wilson, D.J., van de Flierdt, T., McKay, R.M., Patterson, M.O., Jimenez-Espejo, F.J., Escutia, C., Duke, G.C., Taylor-Silva, B.I., Riesselman, C.R., 2018. Pliocene deglacial event timelines and the biogeochemical response offshore wilkes subglacial basin, east antarctica. *Earth and Planetary Science Letters* 494, 109–116.
- Bierman, P.R., Shakun, J.D., Corbett, L.B., Zimmerman, S.R., Rood, D.H., 2016. A persistent and dynamic east greenland ice sheet over the past 7.5 million years. *Nature* 540, 256–260.
- de Boer, B., Haywood, A.M., Dolan, A.M., Hunter, S.J., Prescott, C.L., 2017. The transient response of ice volume to orbital forcing during the warm late pliocene. *Geophysical Research Letters* 44, 10–486.
- Brierley, C.M., Fedorov, A.V., 2010. Relative importance of meridional and zonal sea surface temperature gradients for the onset of the ice ages and pliocene-pleistocene climate evolution. *Paleoceanography* 25.

- 593 Brovkin, V., Brücher, T., Kleinen, T., Zaehle, S., Joos, F., Roth, R., Spahni, R., Schmitt, J.,
594 Fischer, H., Leuenberger, M., et al., 2016. Comparative carbon cycle dynamics of the present
595 and last interglacial. *Quaternary Science Reviews* 137, 15–32.
- 596 Bungum, H., Eldholm, O., 2022. The conundrums of the postglacial tectonic response of the
597 fennoscandian and canadian shields. *Earth-Science Reviews* , 104146.
- 598 Burbidge, D., Gesto, F., Kohn, B., Cummins, P., 2009. Constraints on the current rate of de-
599 formation and surface uplift of the australian continent from a new seismic database and low-t
600 thermochronological data. *Australian Journal of Earth Sciences* 56, 99–110.
- 601 Burke, K.D., Williams, J.W., Chandler, M.A., Haywood, A.M., Lunt, D.J., Otto-Bliesner, B.L.,
602 2018. Pliocene and eocene provide best analogs for near-future climates. *Proceedings of the
603 National Academy of Sciences* 115, 13288–13293.
- 604 Chen, F., Friedman, S., Gertler, C.G., Looney, J., O'Connell, N., Sierks, K., Mitrovica, J.X., 2014.
605 Refining estimates of polar ice volumes during the mis11 interglacial using sea level records from
606 south africa. *Journal of Climate* 27, 8740–8746.
- 607 Conrad, C., Husson, L., 2009. Influence of dynamic topography on sea level and its rate of change.
608 *Lithosphere* 1, 110–120. doi:10.1130/L32.1.
- 609 Crawford, O., Al-Attar, D., Tromp, J., Mitrovica, J.X., Austermann, J., Lau, H.C., 2018. Quan-
610 tifying the sensitivity of post-glacial sea level change to laterally varying viscosity. *Geophysical
611 journal international* 214, 1324–1363.
- 612 Creel, R., Austermann, J., Kopp, R., Khan, N., Ashe, E., Kingslake, J., Albrecht, T., 2022.
613 Probabilistic estimation of mid-holocene global mean sea level, in: EGU General Assembly
614 Conference Abstracts, pp. EGU22–1953.
- 615 Creveling, J.R., Austermann, J., Dutton, A., 2019. Uplift of trail ridge, florida, by karst dissolution,
616 glacial isostatic adjustment, and dynamic topography. *Journal of Geophysical Research: Solid
617 Earth* 124, 13354–13366.
- 618 Dalton, C.A., Wilson, D.S., Herbert, T.D., 2022. Evidence for a global slowdown in seafloor
619 spreading since 15 ma. *Geophysical Research Letters* 49, e2022GL097937.
- 620 Dumitru, O.A., Austermann, J., Polyak, V.J., Fornós, J.J., Asmerom, Y., Ginés, J., Ginés, A.,
621 Onac, B.P., 2019. Constraints on global mean sea level during pliocene warmth. *Nature* 574,
622 233–236.
- 623 Düsterhus, A., Tamisiea, M.E., Jevrejeva, S., 2016. Estimating the sea level highstand during the
624 last interglacial: a probabilistic massive ensemble approach. *Geophysical Journal International*
625 206, 900–920.
- 626 Dutton, A., Carlson, A.E., Long, A., Milne, G.A., Clark, P.U., DeConto, R., Horton, B.P., Rahm-
627 storf, S., Raymo, M.E., 2015. Sea-level rise due to polar ice-sheet mass loss during past warm
628 periods. *science* 349.
- 629 Dutton, A., Lambeck, K., 2012. Ice volume and sea level during the last interglacial. *science* 337,
630 216–219.

- 631 Dyer, B., Austermann, J., D'Andrea, W.J., Creel, R.C., Sandstrom, M.R., Cashman, M., Rovere,
632 A., Raymo, M.E., 2021. Sea-level trends across the bahamas constrain peak last interglacial ice
633 melt. *Proceedings of the National Academy of Sciences* 118.
- 634 Fernandes, V.M., Roberts, G.G., 2021. Cretaceous to recent net continental uplift from paleobiological
635 data: Insights into sub-plate support. *Bulletin* 133, 1217–1236.
- 636 Forte, A.M., Rowley, D.B., 2022. Earth's isostatic and dynamic topography—a critical perspective.
637 *Geochemistry, Geophysics, Geosystems* 23, e2021GC009740.
- 638 Fox-Kemper, B., Hewitt, H., Xiao, C., Aðalgeirsdóttir, G., Drijfhout, S., Edwards, T., Golledge, N.,
639 Hemer, M., Kopp, R., Krinner, G., Mix, A., Notz, D., Nowicki, S., Nurhati, I., Ruiz, L., Sallée,
640 J.B., Slanger, A., Yu, Y., 2021. Ocean, cryosphere and sea level change, in: Masson-Delmotte,
641 V., Zhai, P., Pirani, A., Connors, S., Péan, C., Berger, S., Caud, N., Chen, Y., Goldfarb,
642 L., Gomis, M., Huang, M., Leitzell, K., Lonnoy, E., Matthews, J., Maycock, T., Waterfield,
643 T., Yelekçi, O., Yu, R., Zhou, B. (Eds.), *Climate Change 2021: The Physical Science Basis.*
644 Contribution of Working Group I to the Sixth Assessment Report of the Intergovernmental
645 Panel on Climate Change. Cambridge University Press, Cambridge, United Kingdom and New
646 York, NY, USA, p. 1211–1362. doi:10.1017/9781009157896.011.
- 647 Ghelichkhan, S., Bunge, H.P., 2018. The adjoint equations for thermochemical compressible mantle
648 convection: derivation and verification by twin experiments. *Proc. Roy. Soc. A* 474, 20180329.
- 649 Golledge, N.R., Thomas, Z.A., Levy, R.H., Gasson, E.G., Naish, T.R., McKay, R.M., Kowalewski,
650 D.E., Fogwill, C.J., 2017. Antarctic climate and ice-sheet configuration during the early pliocene
651 interglacial at 4.23 ma. *Climate of the Past* 13, 959–975.
- 652 Grant, G.R., Naish, T.R., 2021. Pliocene sea level revisited: Is there more than meets the eye?
653 *Past Global Changes Magazine* 29, 34–35.
- 654 Hayek, J.N., Vilacís, B., Bunge, H.P., Friedrich, A.M., Carena, S., Vibe, Y., 2020. Continent-scale
655 hiatus maps for the atlantic realm and australia since the upper jurassic and links to mantle flow
656 induced dynamic topography. *Proc. Roy. Soc. A* 476, 20200390. doi:10.1098/rspa.2020.0390.
- 657 Hearty, P., Rovere, A., Sandstrom, M., O'Leary, M., Roberts, D., Raymo, M.E., 2020. Pliocene-
658 pleistocene stratigraphy and sea-level estimates, republic of south africa with implications for a
659 400 ppmv co2 world. *Paleoceanography and paleoclimatology* 35, e2019PA003835.
- 660 Hibbert, F.D., Rohling, E.J., Dutton, A., Williams, F.H., Chutcharavan, P.M., Zhao, C., Tamisiea,
661 M.E., 2016. Coral indicators of past sea-level change: A global repository of u-series dated
662 benchmarks. *Quaternary Science Reviews* 145, 1–56.
- 663 Hoggard, M., Austermann, J., Randel, C., Stephenson, S., 2021. Observational Estimates of Dy-
664 namic Topography Through Space and Time. American Geophysical Union (AGU). chapter 15.
665 pp. 371–411. doi:<https://doi.org/10.1002/9781119528609.ch15>.
- 666 Hollyday, A., Austermann, J., Lloyd, A., Hoggard, M., Richards, F., Rovere, A., . A re-
667 vised estimate of early pliocene global mean sea level using geodynamic models of the
668 patagonian slab window. *Geochemistry, Geophysics, Geosystems* n/a, e2022GC010648.
669 URL: <https://agupubs.onlinelibrary.wiley.com/doi/abs/10.1029/2022GC010648>,

- 670 doi:<https://doi.org/10.1029/2022GC010648>, arXiv:<https://agupubs.onlinelibrary.wiley.com/doi/10.1029/2022GC010648> 2022GC010648.
- 672 Horton, B.P., Kopp, R.E., Garner, A.J., Hay, C.C., Khan, N.S., Roy, K., Shaw, T.A., 2018.
673 Mapping sea-level change in time, space, and probability. *Annual Review of Environment and
674 Resources* 43, 481–521.
- 675 Huppert, K.L., Royden, L.H., Perron, J.T., 2015. Dominant influence of volcanic loading on
676 vertical motions of the hawaiian islands. *Earth and Planetary Science Letters* 418, 149–171.
- 677 Ivins, E., van der Wal, W., Wiens, D., Lloyd, A., Caron, L., 2023. Antarctic upper mantle rheology.
678 Geological Society, London, Memoirs 56, 267–294.
- 679 Kingslake, J., Scherer, R., Albrecht, T., Coenen, J., Powell, R., Reese, R., Stansell, N., Tulaczyk,
680 S., Wearing, M., Whitehouse, P., 2018. Extensive retreat and re-advance of the west antarctic
681 ice sheet during the holocene. *Nature* 558, 430–434.
- 682 Kopp, R.E., Hay, C.C., Little, C.M., Mitrovica, J.X., 2015. Geographic variability of sea-level
683 change. *Current Climate Change Reports* 1, 192–204.
- 684 Kopp, R.E., Simons, F.J., Mitrovica, J.X., Maloof, A.C., Oppenheimer, M., 2013. A probabilistic
685 assessment of sea level variations within the last interglacial stage. *Geophysical Journal
686 International* 193, 711–716.
- 687 Lambeck, K., Rouby, H., Purcell, A., Sun, Y., Sambridge, M., 2014. Sea level and global ice
688 volumes from the last glacial maximum to the holocene. *Proceedings of the National Academy
689 of Sciences* 111, 15296–15303.
- 690 Landais, A., Masson-Delmotte, V., Capron, E., Langebroek, P.M., Bakker, P., Stone, E.J., Merz,
691 N., Raible, C.C., Fischer, H., Orsi, A., et al., 2016. How warm was greenland during the last
692 interglacial period? *Climate of the Past* 12, 1933–1948.
- 693 Lau, H.C., Austermann, J., Holtzman, B.K., Havlin, C., Lloyd, A.J., Book, C., Hopper, E., 2021.
694 Frequency dependent mantle viscoelasticity via the complex viscosity: Cases from antarctica.
695 *Journal of Geophysical Research: Solid Earth* 126, e2021JB022622.
- 696 Lu, C., Forte, A.M., Simmons, N.A., Grand, S.P., Kajan, M.N., Lai, H., Garnero, E.J., 2020. The
697 sensitivity of joint inversions of seismic and geodynamic data to mantle viscosity. *Geochemistry,
698 Geophysics, Geosystems* 21, e2019GC008648.
- 699 Malatesta, L.C., Finnegan, N.J., Huppert, K.L., Carreño, E.I., 2022. The influence of rock uplift
700 rate on the formation and preservation of individual marine terraces during multiple sea-level
701 stands. *Geology* 50, 101–105.
- 702 Miller, K.G., Browning, J.V., Schmelz, W.J., Kopp, R.E., Mountain, G.S., Wright, J.D., 2020.
703 Cenozoic sea-level and cryospheric evolution from deep-sea geochemical and continental margin
704 records. *Science advances* 6, eaaz1346.
- 705 Miller, M.S., Becker, T.W., 2012. Mantle flow deflected by interactions between subducted slabs
706 and cratonic keels. *Nature Geosci.* 5, 726–730. doi:10.1038/ngeo1553.

- 707 Mitrovica, J., Milne, G., 2002. On the origin of late holocene sea-level highstands within equatorial
708 ocean basins. *Quaternary Science Reviews* 21, 2179–2190.
- 709 Mitrovica, J.X., Wahr, J., Matsuyama, I., Paulson, A., 2005. The rotational stability of an ice-age
710 earth. *Geophysical Journal International* 161, 491–506.
- 711 Moucha, R., Ruetenik, G.A., 2017. Interplay between dynamic topography and flexure along the
712 us atlantic passive margin: Insights from landscape evolution modeling. *Global and Planetary
713 Change* 149, 72–78.
- 714 Müller, R.D., Sdrolias, M., Gaina, C., Roest, W.R., 2008. Age, spreading rates and spreading asym-
715 metry of the world's ocean crust. *Geochem. Geophys. Geosys.* 9. doi:10.1029/2007GC001743.
- 716 Murray-Wallace, C.V., Woodroffe, C.D., 2014. Quaternary sea-level changes: a global perspective.
717 Cambridge University Press.
- 718 Pfeffer, J., Spada, G., Mémin, A., Boy, J.P., Allemand, P., 2017. Decoding the origins of vertical
719 land motions observed today at coasts. *Geophysical Journal International* 210, 148–165.
- 720 Pico, T., 2020. Towards assessing the influence of sediment loading on last interglacial sea level.
721 *Geophysical Journal International* 220, 384–392.
- 722 Plach, A., Nisancioglu, K.H., Langebroek, P.M., Born, A., et al., 2019. Eemian greenland ice sheet
723 simulated with a higher-order model shows strong sensitivity to surface mass balance forcing.
724 *The Cryosphere* 13, 2133–2148.
- 725 Polyak, V.J., Onac, B.P., Fornós, J.J., Hay, C., Asmerom, Y., Dorale, J.A., Ginés, J., Tuccimei,
726 P., Ginés, A., 2018. A highly resolved record of relative sea level in the western mediterranean
727 sea during the last interglacial period. *Nature geoscience* 11, 860–864.
- 728 Rachmayani, R., Prange, M., Lunt, D.J., Stone, E.J., Schulz, M., 2017. Sensitivity of the greenland
729 ice sheet to interglacial climate forcing: Mis 5e versus mis 11. *Paleoceanography* 32, 1089–1101.
- 730 Rae, J.W., Zhang, Y.G., Liu, X., Foster, G.L., Stoll, H.M., Whiteford, R.D., 2021. Atmospheric
731 co₂ over the past 66 million years from marine archives. *Annual Review of Earth and Planetary
732 Sciences* 49, 609–641.
- 733 Ramalho, R.S., Helffrich, G., Madeira, J., Cosca, M., Thomas, C., Quartau, R., Hipólito, A.,
734 Rovere, A., Hearty, P.J., Ávila, S.P., 2017. Emergence and evolution of santa maria island
735 (azores)—the conundrum of uplifted islands revisited. *Bulletin* 129, 372–390.
- 736 Raymo, M.E., 1994. The initiation of northern hemisphere glaciation. *Annual Review of Earth
737 and Planetary Sciences* 22, 353–383.
- 738 Raymo, M.E., Kozdon, R., Evans, D., Lisiecki, L., Ford, H.L., 2018. The accuracy of mid-pliocene
739 δ18o-based ice volume and sea level reconstructions. *Earth-Science Reviews* 177, 291–302.
- 740 Raymo, M.E., Mitrovica, J.X., 2012. Collapse of polar ice sheets during the stage 11 interglacial.
741 *Nature* 483, 453–456.
- 742 Raymo, M.E., Mitrovica, J.X., O'Leary, M.J., DeConto, R.M., Hearty, P.J., 2011. Departures from
743 eustasy in pliocene sea-level records. *Nature Geoscience* 4, 328–332.

- 744 Richards, F.D., Coulson, S., Hoggard, M., Austermann, J., Dyer, B., Mitrovica, J.X., 2022. Correcting for mantle dynamics reconciles mid-pliocene sea-level estimates. *EarthArXiv* .
- 746 Richards, F.D., Hoggard, M.J., Ghelichkhan, S., Koelemeijer, P., Lau, H.C., 2023. Geodynamic, geodetic, and seismic constraints favour deflated and dense-cored llvps. *Earth and Planetary Science Letters* 602, 117964.
- 749 Roberts, D.L., Karkanas, P., Jacobs, Z., Marean, C.W., Roberts, R.G., 2012. Melting ice sheets 400,000 yr ago raised sea level by 13 m: Past analogue for future trends. *Earth and Planetary Science Letters* 357, 226–237.
- 752 Rohling, E.J., Hibbert, F.D., Grant, K.M., Galaasen, E.V., Ivali, N., Kleiven, H.F., Marino, G., Ninnemann, U., Roberts, A.P., Rosenthal, Y., et al., 2019. Asynchronous antarctic and greenland ice-volume contributions to the last interglacial sea-level highstand. *Nature Communications* 10, 5040.
- 756 Rovere, A., Ryan, D.D., Vacchi, M., Dutton, A., Simms, A.R., Murray-Wallace, C.V., 2022. The world atlas of last interglacial shorelines (version 1.0). *Earth System Science Data Discussions*, 1–37.
- 759 Tzedakis, P.C., Hodell, D.A., Nehrbass-Ahles, C., Mitsui, T., Wolff, E.W., 2022. Marine isotope stage 11c: An unusual interglacial. *Quaternary Science Reviews* 284, 107493.
- 761 Waelbroeck, C., Labeyrie, L., Michel, E., Duplessy, J.C., Mcmanus, J.F., Lambeck, K., Balbon, E., Labracherie, M., 2002. Sea-level and deep water temperature changes derived from benthic foraminifera isotopic records. *Quaternary science reviews* 21, 295–305.
- 764 Wardlaw, B.R., Quinn, T.M., 1991. The record of pliocene sea-level change at enewetak atoll. *Quaternary Science Reviews* 10, 247–258.
- 766 Watts, A.B., 2001. *Isostasy and Flexure of the Lithosphere*. Cambridge University Press.
- 767 Wright, N.M., Seton, M., Williams, S.E., Whittaker, J.M., Müller, R.D., 2020. Sea-level fluctuations driven by changes in global ocean basin volume following supercontinent break-up. *Earth-Science Reviews* 208, 103293.
- 770 Young, A., Flament, N., Hall, L., Merdith, A., 2021. The influence of mantle flow on intracontinental basins: Three examples from Australia. *Basin Research* 33, 1429–1453.
- 772 Young, A., Flament, N., Williams, S.E., Merdith, A., Cao, X., Müller, R.D., 2022. Long-term phanerozoic sea level change from solid earth processes. *Earth and Planetary Science Letters* 584, 117451.

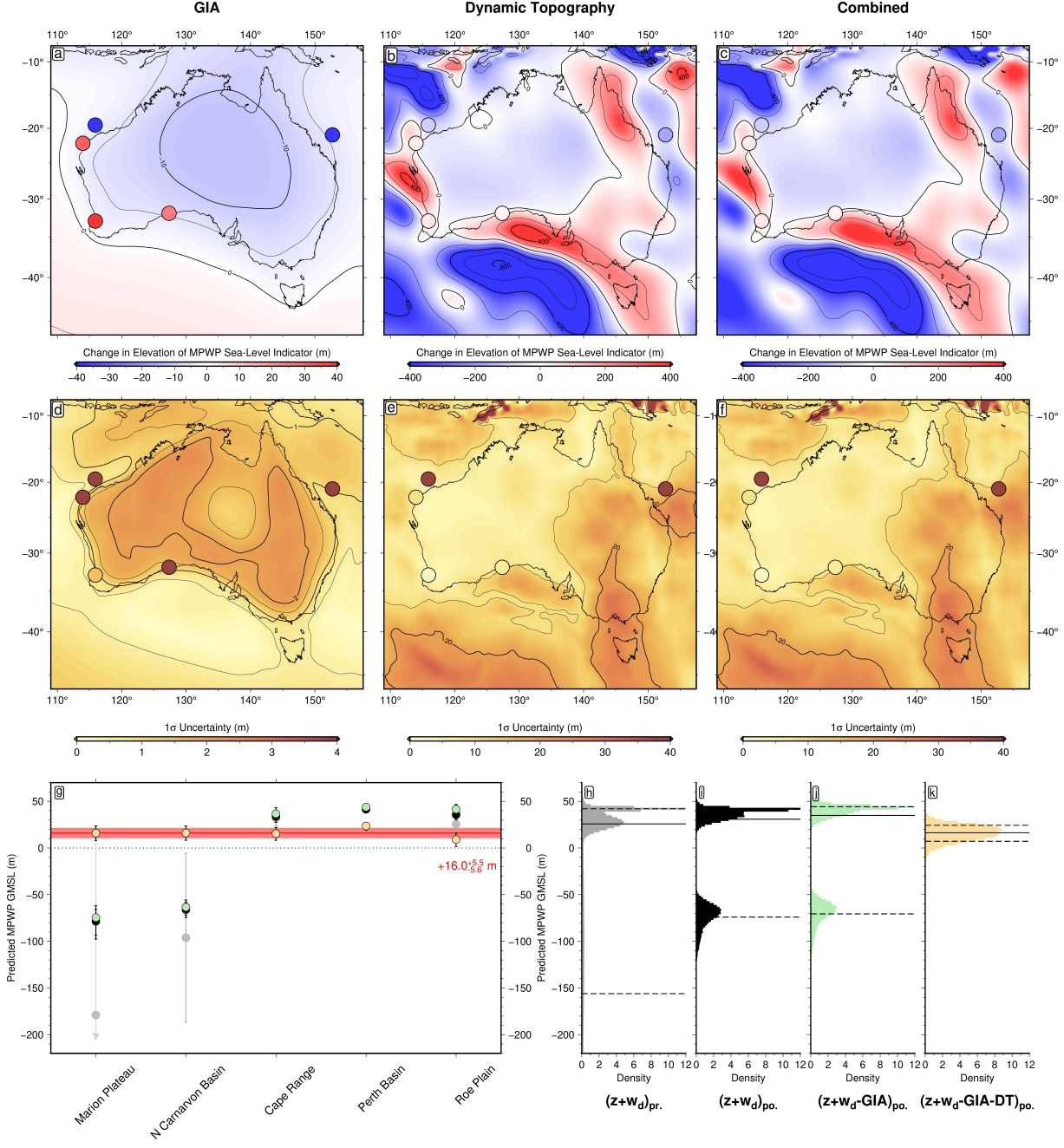


Figure 3: Correcting Australian MPWP relative sea-level markers for mantle dynamics. (a) GIA-induced change in MPWP sea-level marker elevation. Background colour = posterior median of 3 Ma–Recent GIA-induced relative elevation change. Circles = prior median of uncorrected 3 Ma GMSL estimates (i.e., present-day elevation (z) + palaeo-water depth (w_d)). (b) Same for dynamic topography (DT). (c) Same for combined GIA and DT contribution. (d) Uncertainty on predicted elevation change. Background colour = posterior 1σ uncertainty of 3 Ma–Recent GIA-induced relative elevation change. Circles = prior 1σ uncertainty of uncorrected 3 Ma GMSL estimates. (e) Same for DT. (f) Same for combined GIA and DT contribution (g) DT- and GIA-corrected 3 Ma GMSL along transect anti-clockwise from Cape Range. Yellow circles and error bars = 50^{th} and $16^{\text{th}}\text{--}84^{\text{th}}$ percentiles of DT- and GIA-corrected posterior distribution. Grey/black/green circles and error bars = same for uncorrected prior/uncorrected posterior/GIA-corrected posterior distribution. (h) Histogram of uncorrected 3 Ma GMSL prior distribution; solid/dashed lines = $50^{\text{th}}/16^{\text{th}}\text{--}84^{\text{th}}$ GMSL percentiles. (i) Same for uncorrected posterior distribution. (j) Same for GIA-corrected posterior distribution. (k) Same for DT- and GIA-corrected posterior distribution.

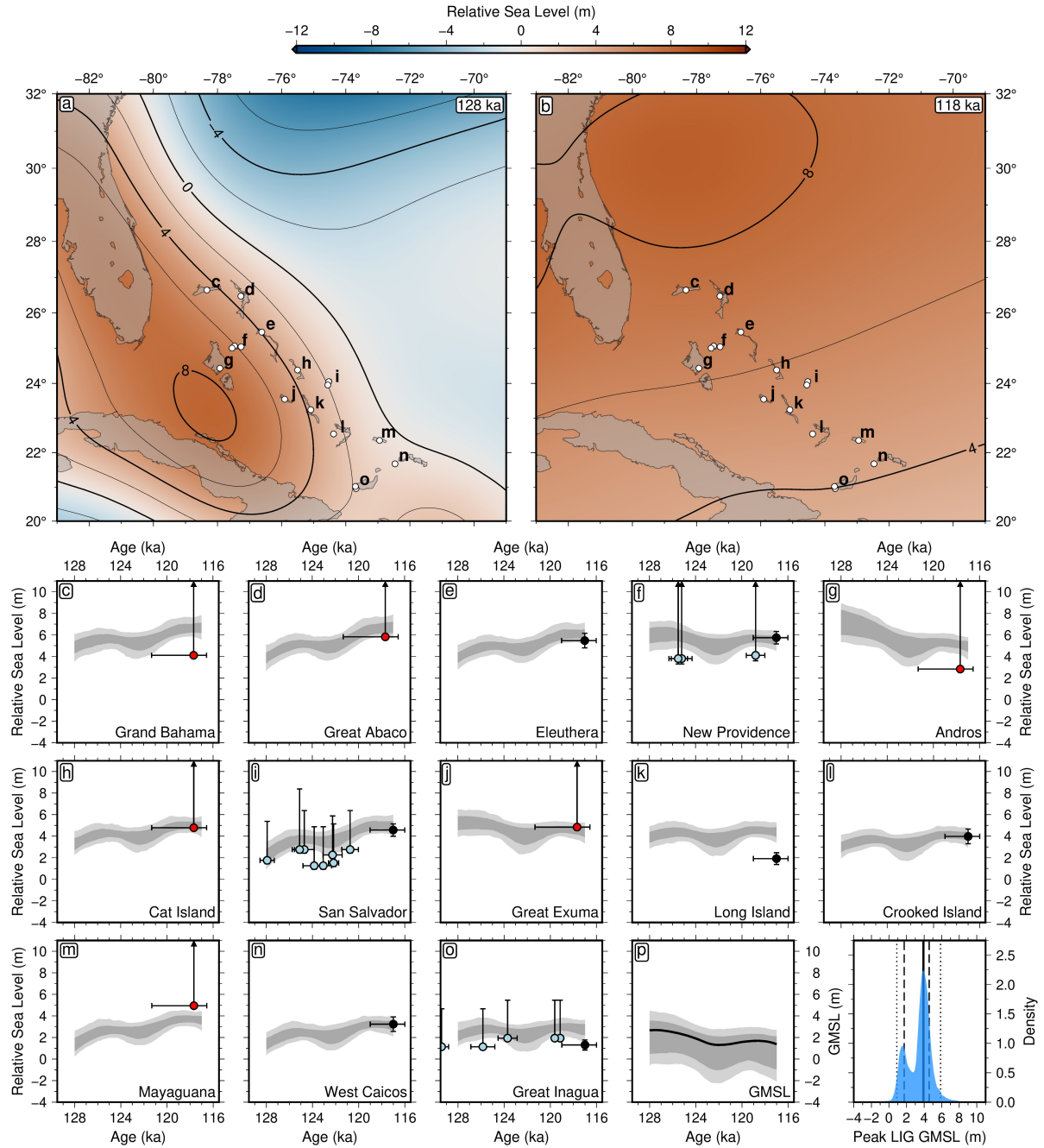


Figure 4: Probabilistic estimation of LIG GMSL from GIA-corrected Bahamian RSL records (redrawn with permission from Dyer et al., 2021). (a) RSL at 128 ka from maximum likelihood GIA model (assumes 96 km thick elastic lithosphere, 0.5×10^{21} Pa s/ 40×10^{21} Pa s upper/lower mantle viscosities, an MIS 6 Laurentide Ice Sheet containing 66 m GMSLE, and the Waelbroeck et al. (2002) GMSL curve). White circles = loci of LIG sea-level indicators. Labels correspond to island sites in panels c–m. (b) RSL at 118 ka. (c–m) Site-specific LIG RSL trends. Red circles = marine highstands; blue circles = corals; black circles = beach deposits (ordinary berms); light/dark gray bands = central 68%/95% of inferred posterior distribution. (n) Inferred LIG GMSL trend. Solid line = most likely GMSL trend (maximum *a posteriori* [MAP] probability estimate). (o) Inferred posterior distribution of peak GMSL. Dotted lines = 2.5th/97.5th percentiles (0.9 m/5.9 m); dashed lines = 16th/84th percentiles (1.7 m/4.6 m); solid line = MAP estimate (3.9 m).

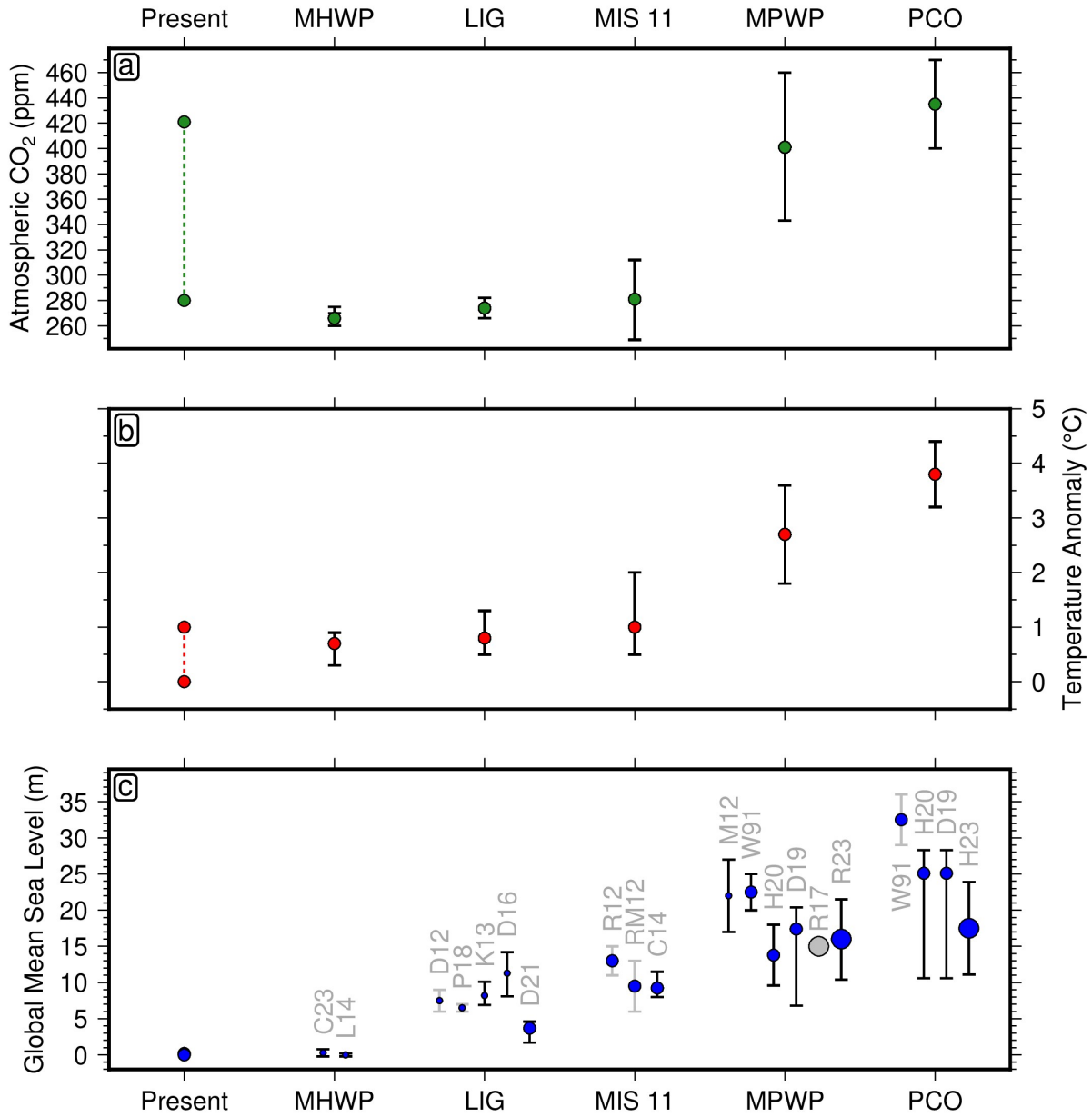


Figure 5: Summary of climatic variables during key warm periods. (a) Atmospheric CO₂ (Brovkin et al., 2016; Rae et al., 2021). Dotted lines connect between pre-industrial and present-day conditions. (b) mean global surface temperature (Burke et al., 2018; Rachmayani et al., 2017; Tzedakis et al., 2022; Brierley and Fedorov, 2010). (c) GMSL. Grey symbol/blue with grey error bar/blue with black error bar = no/limited/comprehensive uncertainty quantification; small/medium/large symbol = uncorrected/indirectly corrected/directly corrected for dynamic topography-induced RSL changes. C23 = (Creel et al., 2022); L14 = (Lambeck et al., 2014); D12 = (Dutton and Lambeck, 2012); P18 = (Polyak et al., 2018); K13 = (Kopp et al., 2013); D16 = (Düsterhus et al., 2016); D21 = (Dyer et al., 2021); R12 = (Roberts et al., 2012); RM12 = (Raymo and Mitrovica, 2012); C14 = (Chen et al., 2014); M12 = (Miller and Becker, 2012); W91 = (Wardlaw and Quinn, 1991); H20 = (Hearty et al., 2020); D19 = (Dumitru et al., 2019); R17 = (Moucha and Ruetenik, 2017); R23 = (Richards et al., 2022); H23 = (Hollyday et al.).